Ice-stream-related patterns of ice flow in the interior of northeast Greenland

M. A. Fahnestock,[1] I. Joughin,[2] T. A. Scambos,[3] R. Kwok,[2] W. B. Krabill,[4] and S. Gogineni[5]

Abstract. Ice flow in the interior of the NE quadrant of the Greenland ice sheet is focused on the large ice stream draining the north side of the summit dome. The rapid ice flow in the stream is apparent in the surface features in the stream and at the margins, in the broad scale topography that drives ice flow, and in satellite-derived ice motion information. The patterns of ice flow in the upper half of the stream are remarkable for their level of organization, simple geometry, and effects on local surface topography. The stream begins less than 100 km from the ice divide as a current 15 km wide and then broadens symmetrically downstream by the addition of ice from the sides to a width of more than 60 km. Elevation data and visible-band imagery show that the stream has marginal troughs tens of meters deep in its upper reach which are coincident with regions of high shear strain rate. The topography of the margins and undulating surface of the stream is generated by the ice flow; the surface undulations in the stream are fixed in location and shape over the 5 year period from 1994 to 1999. The enhanced flow presents a challenge for researchers trying to understand the history of ice discharge from a significant area in the interior of the ice sheet.

1. Background

Although the Greenland ice sheet is drained by a number of rapidly flowing outlet glaciers which achieve high flow rates within a few hundred kilometers of the coast, the pattern of slow deformational ice flow in the deep interior is interrupted by the presence of an ice stream, or rapidly flowing current, only in the northeast. Jakobshavn Isbrae, in central west Greenland, the best known of Greenland's outlet glaciers, shows organized flow in satellite imagery only 100 km inland from the grounding line. The ice stream in the northeast, in contrast, is a nearly straight feature about 700 km long, with identifiable margins for most of its length and a topographically undulating interior due to the rapid ice flow. Ice streams of similar size are conduits for rapid discharge from West Antarctica [e.g., *Bentley*, 1987] and are thought to have a role in any potential instability of that ice sheet.

Though extensive, the ice stream is difficult to view from an aircraft or on the surface; it has been crossed several times by traverse parties, but the effects of the rapid flow were noticed only in isolated locations. The British North Greenland Expedition had trouble with crevasses on the tops of surface undulations just out from Farewell Nunatak. M. Fahnestock observed these undulation-top crevasses as far upstream as 77.3°N, 30°W on a flight in 1995.

The stream does not have a proper designation, having been referred to as the "northeast Greenland ice stream" in previous descriptions [*Fahnestock et al.*, 1993; *Ekholm et al.*, 1998;

Joughin et al., 1997]. We propose the name "Brønlund ice stream" after Jørgen Brønlund, a well-known Greenlandic figure from the early phase of scientific exploration in the north. He perished near Nioghalvfjerdsfjorden, while on the Mylius-Erichsen expedition mapping the unknown area north of Danmarkshavn. On this expedition the traverse party passed all of the major outlet glaciers fed by the ice stream. We will submit this name for consideration to appropriate authorities in Greenland and Denmark.

This paper is a companion to the paper by *Joughin et al.* [this issue], which discusses an interferometrically derived velocity field for ice flow in this quadrant, the state of balance of the stream given measured accumulation rates and ice flow speeds, and model-based inversion of the flow data for basal stresses. We will discuss the appearance of the stream in several data sets, emphasizing what these data tell us about the stream in its upper reaches. We will look in detail at the patterns of ice flow and the impact of the flow in the stream on the surface topography of the ice sheet.

2. Data

The stream is most effectively observed with satellite-based techniques. We will describe what is known about the stream from a combination of satellite images, interferometric displacement measurements from imaging radar (INSAR), an elevation model derived from radar altimetry measurements and slope from visible imagery, and aircraft-based laser altimetry and ice-penetrating radar profiles. These data were collected and compiled by a number of investigators. The interferometrically derived velocity field is described in two papers by *Joughin et al.* [this issue, 1996]. Radar altimetry measurements of Greenland were compiled into a digital elevation model (DEM) by *Ekholm et al.* [1995, 1998] and *Bamber* [this issue]. This elevation field has been enhanced in fine detail using AVHRR photoclinometry [*Scambos and Fahnestock*, 1998; *Scambos and Haran*, in press]. Aircraft-based laser altimetry profiles [*Krabill et al.*, 2000] and ice-penetrating radar [*Gogineni et al.*, 1998; *Legarsky et al.*, 1998] were collected as part of the NASA Program for Arctic Regional Climate Assessment (PARCA).

3. Ice Stream Morphology

3.1. Upper Reach – Start of Organized Flow

The ice stream was first described from its appearance in ERS-1 synthetic aperture radar (SAR) imagery and visible-band satellite imagery [*Fahnestock et al.*, 1993]. This imagery reveals fine structure in the margins of the stream, and provides an indication of undulating topography in the interior. *Ekholm et al.* [1998] pointed out the appearance of the ice stream in a radar-altimetry-based elevation model, noting the undulating surface which differed from the surrounding ice, and also showed that some surface undulations were located over variations in bed topography.

The ice stream is distinctly visible in the surface topography of the ice sheet far into the interior, first identifiable as a 15 km wide feature with subtle troughs along its margins just below the 3,000 m elevation contour. Figure 1 provides two representations of the topography associated with the interior of the ice stream. Figure 1a is a grayscale representation of the high-frequency component of the topography, showing surface undulations, ridge crests, and other features related to ice flow, and Figure 1b is a contoured representation of the regional topography showing the summit dome and the subtle convergence of the topography in the northeast on the axis of the ice stream. The elevation model is derived from radar altimetry [*Ekholm et al.* 1995; *Bamber et al.*, this issue] and enhanced in detail at spatial scales of 1-5 km with slope information extracted from multiple AVHRR images [*Scambos and Fahnestock*, 1998].

The smooth shape of the summit dome can be seen at the bottom of Figure 1b, in distinct contrast to the disturbed topography on the north flank of the dome that reaches an elevation of 3160 m. This region of higher-amplitude (± 15-20 m) surface undulations lies to the east of the first appearance of the stream. In Figure 1a the top half of the ice stream stands out clearly due to dark (low) margins and high-amplitude surface undulations within the stream. The elevation model clearly shows the organized nature and impact of the rapid ice flow in the stream, and the apparently simple geometry of this large feature in its upper reach. We will discuss this topography in relation to the ice flow that produces it in a later section.

The highest-elevation indication of organized flow in the ice stream is the faint northwestern margin above point A in Figure 1a, at an elevation of 2940 m, just under 100 km northeast and 100 m below the closest point on the ice divide, which runs along the northwest ridge of the summit dome. Immediately below the appearance of organized flow, the stream takes the form of a 15 to 20 km wide current for the next 100 km. Below this narrow reach there is a nearly symmetric widening of the stream, which starts with an outward step in the northwestern margin and a simple bend in the southeastern margin. This wedge-shaped widening section of the stream is 80 km long. Downstream of this point, the stream is 60 km wide.

3.2. Coastal Reach

As it reaches the coast, the flow in the stream separates into two branches, which contribute much of the ice discharged into
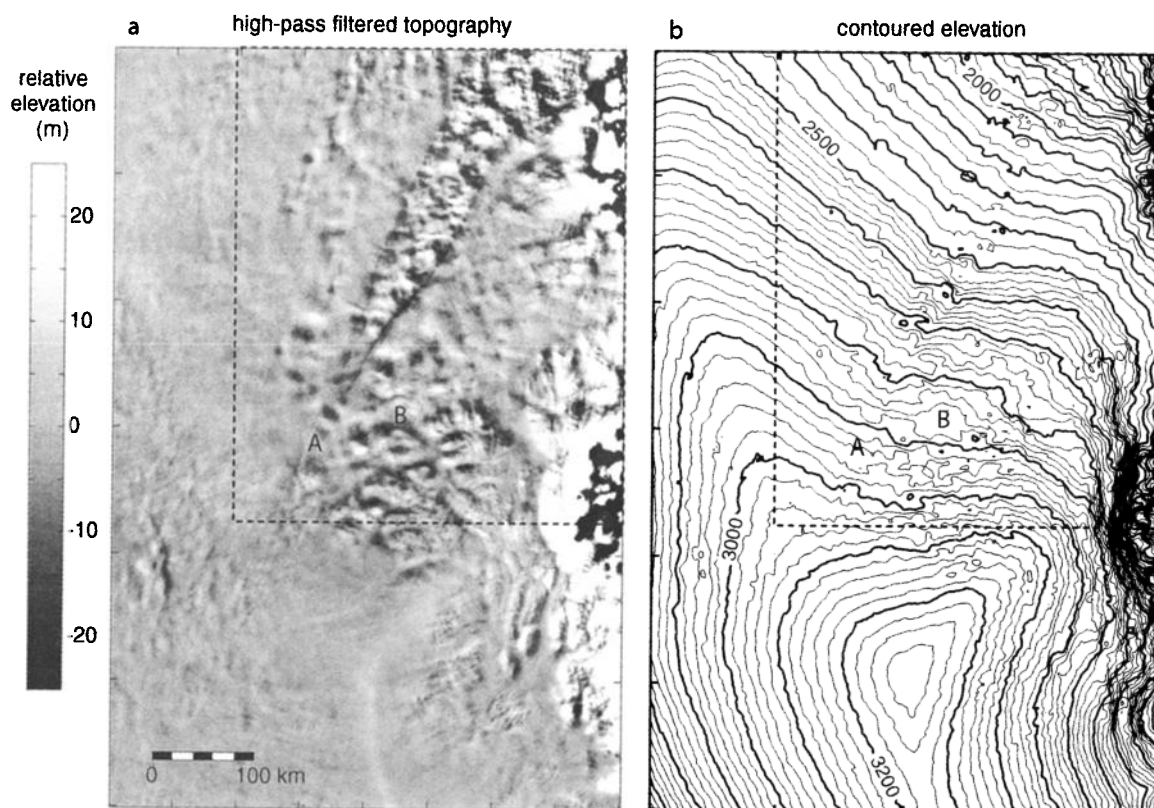

Figure 1. Two representations of the detailed surface topography of a 400 km by 600 km section of the northeastern quadrant of the Greenland ice sheet, showing the topographic expression of the ice stream. The sources of the elevation data are discussed in the text. (a) A gray scale representation of the high-pass-filtered topography, showing deviations from a mean surface calculated with a 50 km radius Gaussian filter. (b) The contoured elevation. Contour intervals are 100 m for wide contours and 20 m (above 2500 m elevation) and 50 m (below 2500 m elevation) for thin contours. The dashed box in each figure outlines the area of overlap with Plate 1b. The points labeled A and B are discussed in the text.
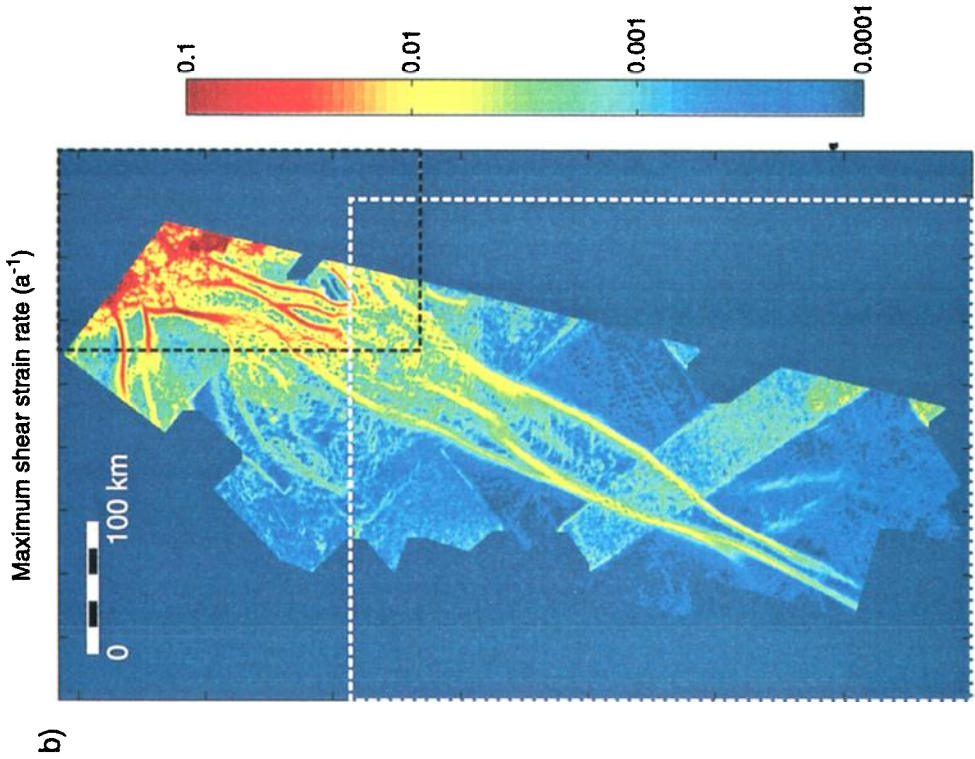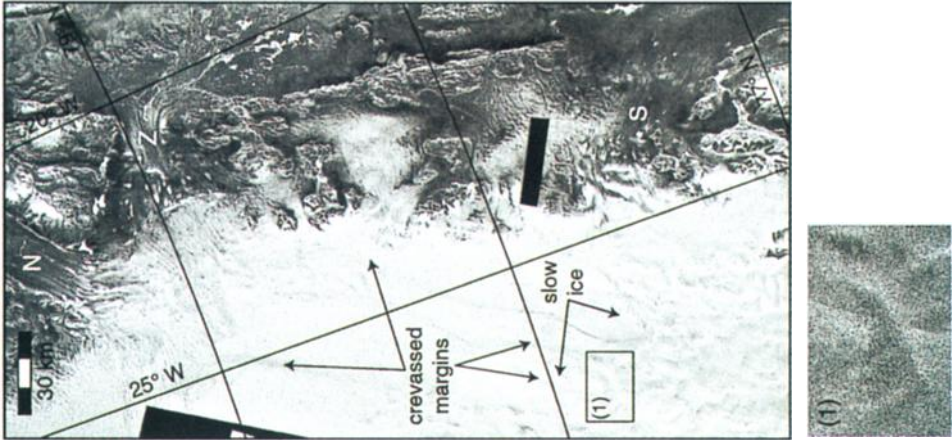
Plate 1. Ice stream margins as imaged with synthetic aperture radar (SAR). (a) A mosaic of SAR images showing the coastal reach of the ice stream (SAR imagery ©ESA 1993). The dark bands show the locations of significant crevassing along the margins in this reach. The inset 1 shows the crevasses visible at 100 m resolution. (b) Maximum shear strain rates calculated from the velocity field of *Joughin et al.* [this issue] on a $\log_{10}$ color scale, highlighting the rapid shearing responsible for the margins visible in the SAR mosaic and in the elevation data of Figure 1. The black dashed box outlines the area covered by the SAR mosaic in Plate 1a; the white dashed box outlines the area of overlap with Figure 1.

the Fram strait between 76° and 79°N (Plate 1a). The branches are formed where the ice flow divides around several slow-moving high points identified in Plate 1a. For the next 150 km downflow on the northern branch, the shear margins that develop at the edges of the flow appear as dark bands in the SAR imagery (Plate 1a). The dark bands correspond to extensive open or snow-filled crevasses that have been observed from aircraft in several places. The ice stream ultimately discharges through three major outlet glaciers. The southern branch flows out Storstrømmen(S in Plate 1a), where the flow turns to the south along the coast. The northern branch contributes all of the ice flowing out Zachariæ/ Isstrøm, (Z in Plate 1a) which narrows as it flows through a fjord and then widens into an ice shelf, and the ice flowing out the southern part of Nioghalvfjerdsfjorden (N in Plate 1a), which also has significant input from ice that originates farther north in the interior. Ice flow has been measured in these glaciers using interferometry [Rignot et al., 1997; Mohr et al., 1998].

4. Ice Stream Margins

The ice stream margins are the zones of rapid shearing immediately adjacent to the slower-moving ice of the ice sheet. Raymond [1996] divided the margin into a narrow outboard stress accommodation zone and a wider inboard stress relaxation zone at the location of maximum shear strain rate. In his models the shear strain rate maximum was slightly inboard of the no-slip/slip transition at the bed. The extensively studied ice streams on the Siple Coast of West Antarctica begin far inland as a series of tributaries, many flowing in deep channels in the bed but having little surface expression [Bindschadler et al., 2000; Joughin et al., 1999; Hodge and Doppelhammer, 1996]. Upon reaching a location that may be defined by a change in bed conditions, the ice flow in these streams accelerates, and discrete margins become visible, defined by their linear character and extensive chaotic crevassing [e.g., Vornberger and Whillans, 1990; Whillans and van der Veen, 1993]. These margins appear when the ice flow speeds in the stream approach 100 m/yr.

The ice stream in northeast Greenland bears some similarity to the ice streams in West Antarctica but in its upper reach shows a number of contrasts. The tributary section of this ice stream is less than 100 km long, if it is defined as the area of convergence above the first appearance of discrete margins. The limited drainage basin of the stream and the converging region above the onset are shown by Joughin et al. [1997, Plate 1]. The ice stream begins as a single linear current of enhanced flow with discrete margins within 100 km of the present ice divide. The margins in this area are narrow linear features in SAR imagery, AVHRR imagery, and SPOT imagery. In the visible band these features appear because they are defined by surface topography. In SAR imagery they appear due to changes in snow conditions, as discussed below.

The margins evolve downstream as the patterns of ice flow change. The stream margins, which are distinct shallow furrows for the uppermost 300 km, change character to more diffuse, less easily defined regions in the undulating topography within and outside of the lower part of the stream. It is not until flow divides around several slow-moving areas above Storstrømmen that crevassed margins resembling the chaotic zones of the West Antarctic ice streams first appear, at ice flow speeds over 100 m/yr.

Figure 1a shows the topographic expression of the marginal troughs in the interior, while Plate 1a shows the dark bands of extensive crevassing in a SAR mosaic of the coastal reach [Fahnestock et al., 1993]. Both features are generated in the high shear strain rate environment of the stream margins as measured by SAR interferometry, as shown by Plate 1b, which is a map of the maximum shear strain rates derived from the velocity map of Joughin et al. [this issue]. The topographic troughs in the interior coincide with regions experiencing shear strain rates of between

0.007 and 0.01 a^{-1}, while the heavily crevassed margins in the lower reach are forming at shear strain rates approaching 0.1 a^{-1}. The rates in the lower margins are comparable to the rates observed in the chaotic zones of the margins of Ice Stream B, West Antarctica, by Echelmeyer et al. [1994] and discussed by Jackson and Kamb [1997].

5. Ice Motion

Ice flow has been measured for the entire ice stream using SAR interferometry, tied to GPS measurements and balance velocities calculated for slow-moving areas removed from the stream. For a complete discussion of the techniques, and a model-based analysis of ice flow in the stream, see Joughin et al. [this issue]. Here we will discuss the details of ice flow patterns in the interior as they relate to flow-related features observed in satellite imagery.

5.1. Onset

As we have discussed, based on the enhanced elevation model, the flow in the onset region begins within 100 km of the ice divide. In the interferometrically derived velocity field of Joughin et al. [this issue] the flow in the onset region appears to be well organized in a single channel at the highest elevations covered by the interferograms. The flow speed increases monotonically downstream, reaching speeds of hundreds of meters per year. Figure 2a shows the magnitude of the rapid ice flow in the interior, and the locations of the velocity and strain-rate profiles presented in Figure 2b. Defining the "start" or "onset" of the rapid ice motion from the INSAR velocity measurements is difficult because organized flow of 10 m/yr is visible in the interferometry to the most upstream point of the coverage. There is a distinct jump in the ice flow speed just below profile 2, where flow speeds increase from just over 10 m/yr to more than 30 m/yr in about 20 km. This rapid increase in flow speed may represent a transition in flow style, although we have limited information about basal conditions in this area. A southern region of enhanced flow speed comes directly off the northern side of the summit dome and joins the stream at the beginning of the widening section (profiles 4 and 5). There are several relatively flat areas in the topography that appear to be associated with the changes in flow speed. One small flat area is just upstream of the area of interferometric coverage (point A in Figure 1, which is the point we also identified as the uppermost expression of organized flow in Figure 1a), and the other somewhat larger area is at the upper end of the southern area of enhanced flow (point B in Figure 1). Both areas have 20 to 40 m high steeper slopes immediately upstream (see contours in Figure 1b). Both are suggestive of locally enhanced sliding at the bed and may be possible sites of onset of rapid flow.

5.2. Wedge-Shaped Widening Section

The wedge-shaped widening of the stream just below the onset region is remarkable for its near symmetry, and for the well-defined narrow margins that appear in the surface topography (Figure 1), in measured shear strain rates (Plate 1b and Figure 2), and in visible-band and SAR imagery (Plate 2). We have traced the paths of ice particles through the interferometric velocity field for this region and can show that the widening is accomplished entirely through the incorporation of ice from the sides into the rapid flow (see Plate 3a). The flow lines within the stream do not diverge with the widening of the margins but rather show a slight convergence as the ice speed increases at the start of the widening section. The rest of the widening is accomplished without significant change in speed (see Figure 2b, profiles 5 through 8), entirely by the addition of ice across the margins.
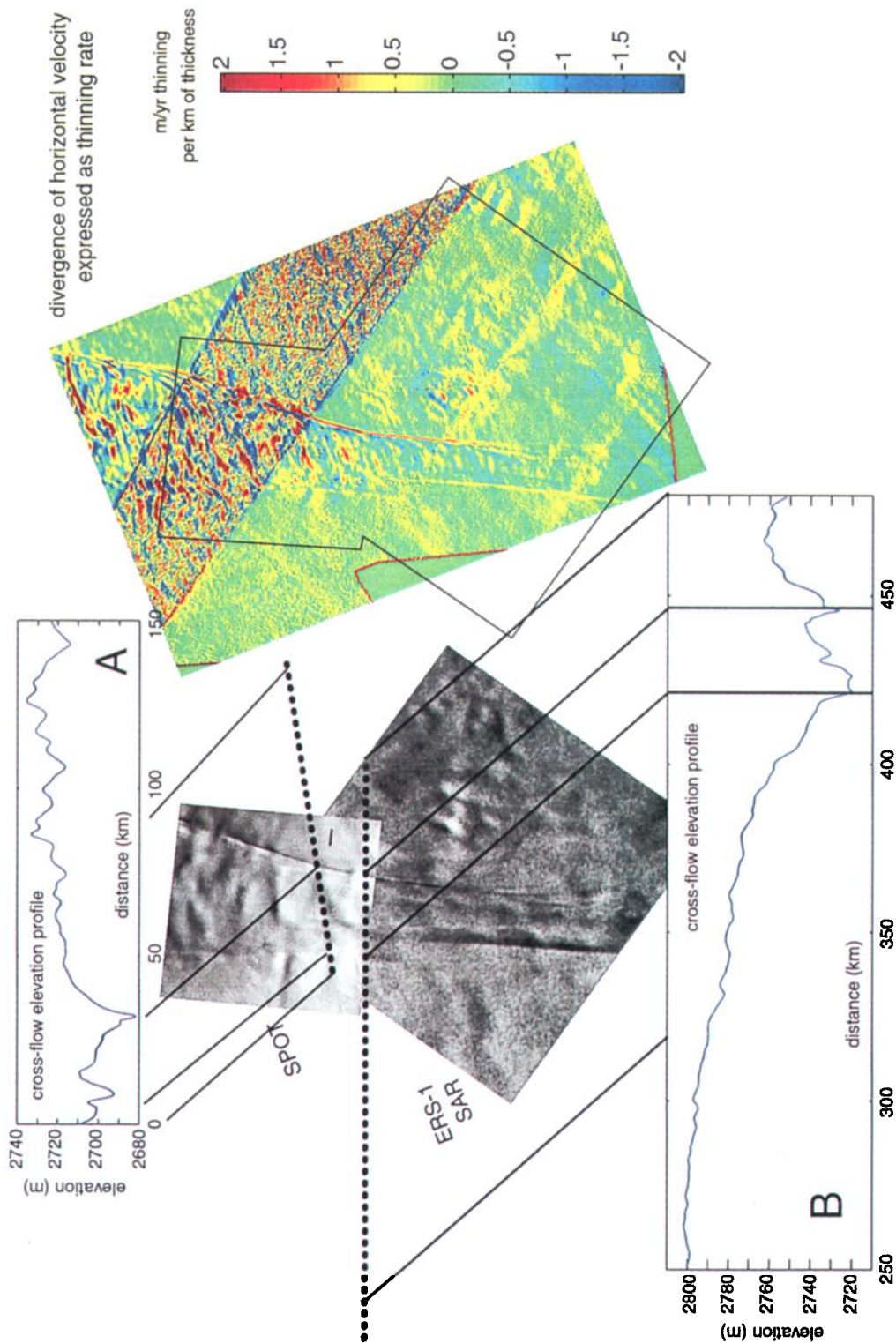
Plate 2. A collection of information about the margins in the upper reach of the ice stream. Profiles A and B are detailed views of the surface topography along two laser altimeter flight lines crossing the upper part of the ice stream. High-resolution visible-band (SPOT) and SAR images showing the narrow marginal troughs underlay the dashed altimeter flight lines. The color image shows the rate of thinning calculated from the divergence of the INSAR velocity field, as discussed in the text. The thinning rate is expressed in meters per year of thinning per kilometer of involved ice thickness, which is equivalent to vertical strain rate x 10^3.
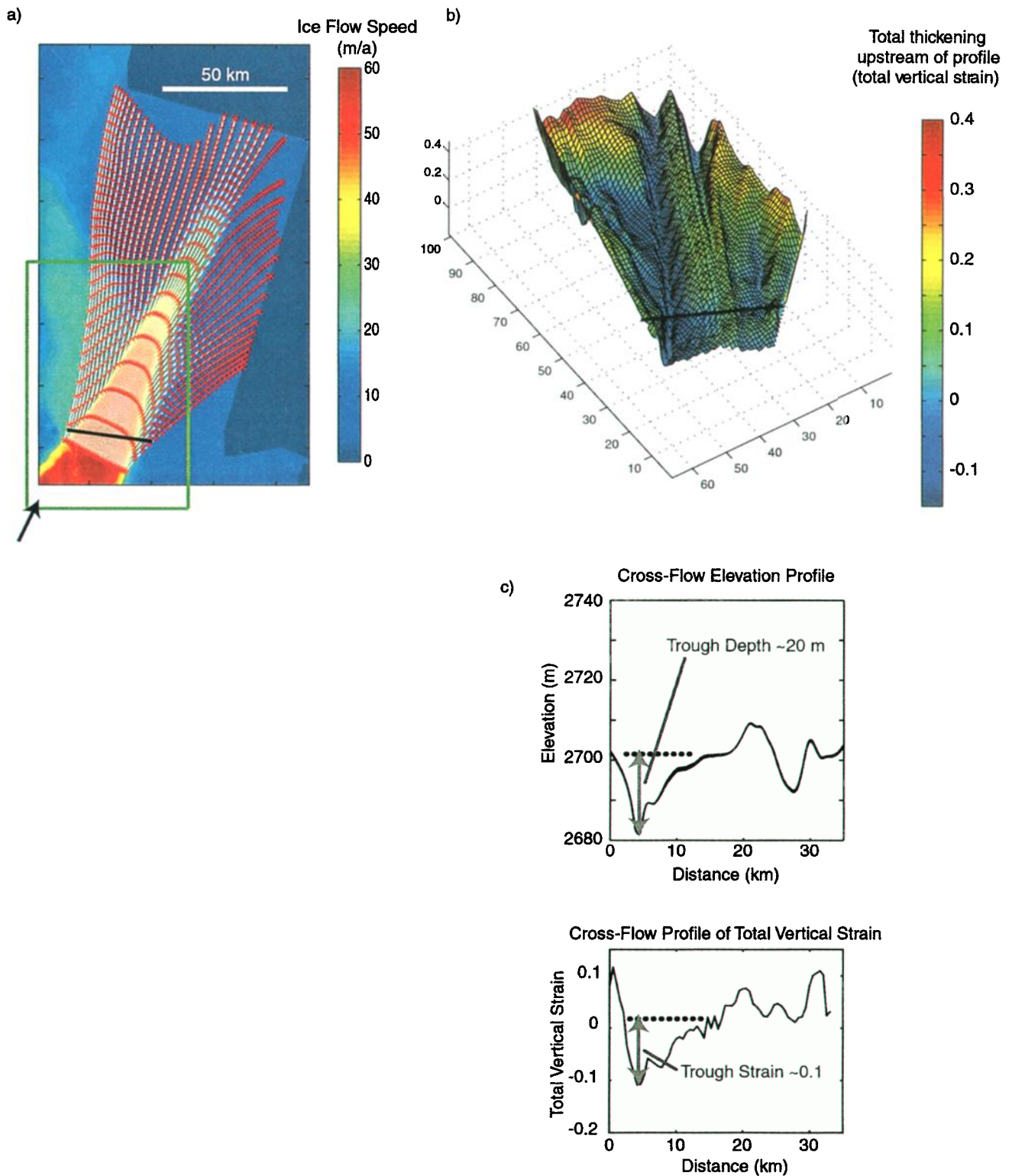
Plate 3. Estimation of the topography generated by ice flow at the start of the wedge-shaped widening section. (a) Flow lines through the INSAR velocity field, labeled with 250 year displacement markers along the trajectories. (b) A three-dimensional representation of the total strain (thickening positive) calculated from the downstream end of the flow lines in Plate 3a by integrating the thinning rates shown in Plate 2. The plate is oriented with the viewing direction indicated by the black arrow. The horizontal axes cover the region outlined by the green box in Plate 3a, while the vertical axis is in units of total vertical strain. (c) Laser altimeter profile (from Plate 2, profile A) over the black line, showing the ~20 m depth of the trough, and the cross-flow profile of total strain over the same region, showing the -0.1 total strain which defines the trough.
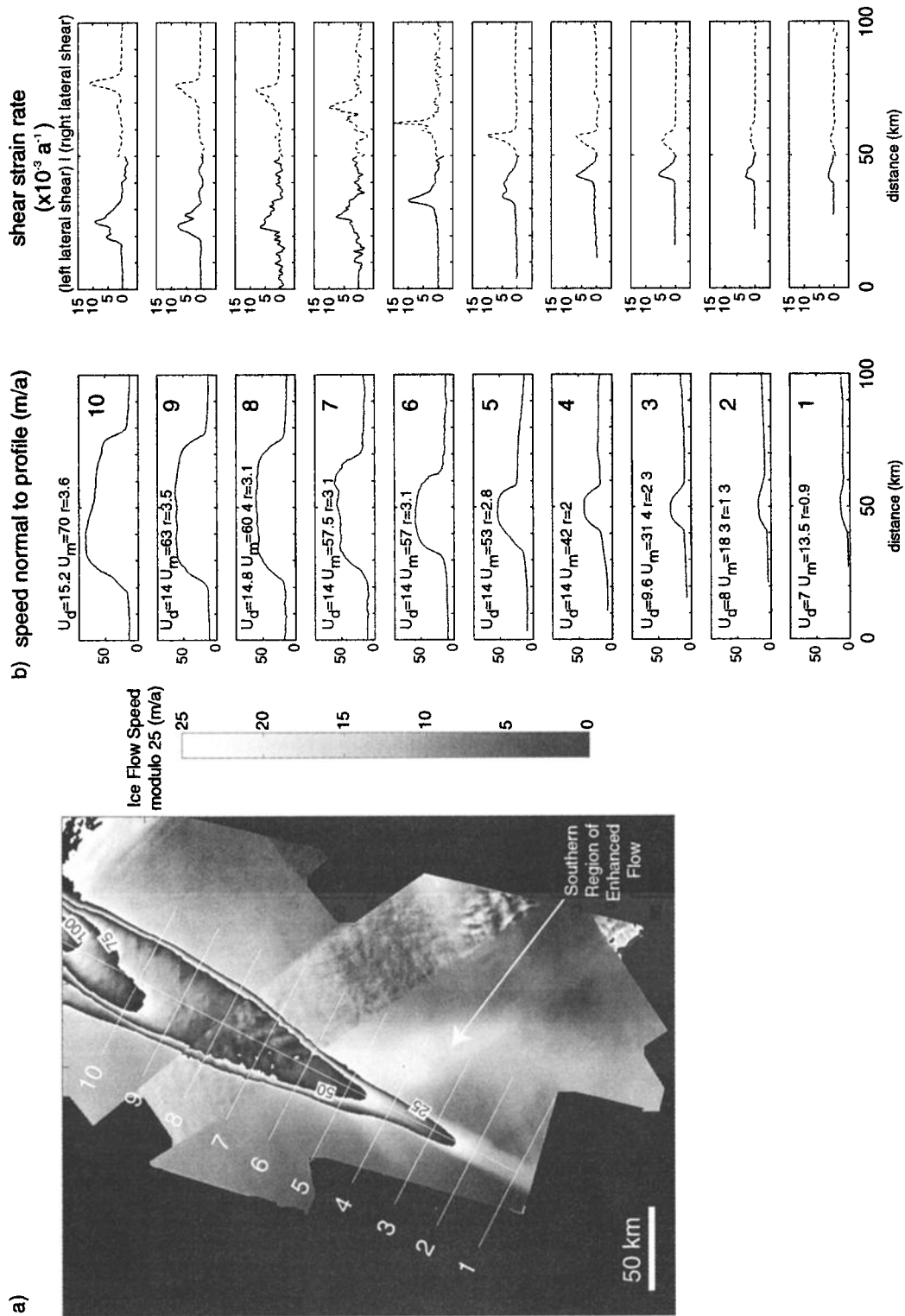
Figure 2. (a) Locations of the 10 profiles plotted in Figure 2b, overlain on the INSAR-derived velocity field of the onset region. The ice flow speed is shown as a gray scale cycle for each 25 m/yr increment; each white/black transition is labeled with the speed at that transition. This method of display is used so that the subtle variations in speed are apparent. The labeled region of enhanced flow is discussed in the text. (b) Ice flow speeds normal to the profiles in Figure 2a and the shear strain rates across those profiles. Shear strain rate is plotted with a sign change at the centerline, so both margins show positive rates of shear. The values u_d, u_m, and r are discussed in the text.

5.3. Changes in Flow Style

Joughin et al. [this issue] use a model-based inversion of the velocity field and conclude that in the narrow upper reach there is very little resistance at the bed; but that further downstream, the bed provides a significant fraction of the resistance to ice flow. Figure 2 shows this evolution in flow style along the ice stream using regularly spaced profiles of ice flow speed and shear strain rate.

The cross profile of flow in the onset area is parabolic, with a rapid rise in shear strain rate at the margins followed by a slower but still linear decline in shear strain rate toward the center. The initial rise in shear stain rates as one moves toward the stream reflects a region of accommodation where marginal shear stress is transferred to the bed, which *Raymond* [1996] found from theoretical considerations to have a width of the order of an ice thickness. His analysis also showed that the drop in strain rate toward the center of the stream defined a region of influence with a width that depended on the ratio of internal deformation to basal sliding and the properties of the ice. We make a crude estimate of the amount of surface motion due to internal deformation by taking the average of the flow speed on a profile outside of the stream (the flow in the cross-profile direction u_d) and approximate Raymond's slip ratio as

$$r \approx \frac{\left(u_m - u_d\right)}{\left(u_d\right)}, \qquad (1)$$

where (u_m) is the maximum centerline speed. This estimate of internal deformation velocity u_d is reasonable to a rough approximation because the surface slope in the cross-profile direction and the ice thickness are both close to their values in the stream. The slip ratio (shown for each profile in Figure 2b) ranges from 0.9 in profile 1 to 3.6 in profile 10. These values are significantly lower than the range of $10^1 - 10^7$ considered by Raymond but are comparable to the 10^1 case. In his analysis, this low value of the slip ratio leads to narrow shear margins comparable to the widths we see in the interferometric velocity measurements.

We would argue that in the onset region, enhanced flow in the stream is due to basal sliding, based on the observation that flow at the centerline is still within the zone of influence of the side shear; this is not surprising given a zone width that is typically of the order of 3 times the ice thickness (3 x 3000 m in this area). Similar comparisons can be made with the results of *Echelmeyer et al.* [1994].

The cross profile of flow in the wedge-shaped widening section evolves rapidly to become plug-like, a condition that continues for some distance downstream. Through this section (profiles 4-9 in Figure 2) the cross profile of flow speed changes from a nearly parabolic character to a flat-centered profile with shear concentrated near the margins. The shear strain-rate profiles through this section evolve as well, although the width of the shear margins does not increase significantly with increasing stream width until the northwestern margin begins to spread between profiles 9 and 10. The broad regions of very low shear strain rates in the stream interior and the irregular nature of the shear strain rates in the interiors of profiles 7 through 10 suggest that local basal drag has an effect on determining ice flow speed. The change to a more plug-like flow style may reflect an increasing total driving force as the stream widens, while the shear margins maintain similar widths and shear strain rates, and therefore similar lateral stress transfers (if there is no significant softening).

The plug flow returns over about 50 km to a more parabolic flow profile in the northwestern half of the stream (profiles 8, 9 and 10), but with a different shear strain-rate pattern than that seen in the onset area. In profile 10 the shear strain rate on the northwestern (left hand) side is distributed across this part of the stream, while the shear strain rate on the southeastern margin is very high and more concentrated than on any other profile. This

change in character reflects a change in the flow associated with a channel that is developing in the bed on the northwestern side of the stream. The speed along the flow centerline nearly doubles with this change in flow character, from about 60 m/yr at profile 8 to over 100 m/yr 50 km downstream of profile 10, while the centerline of the rapid flow moves first to the left-hand side of the stream, then curves to the right across the stream as the head of Storstrømmen (S in Plate 1a) is approached.

Although the margins in the upper half of the ice stream are distinct in visible-band and SAR imagery, and the extensional strain rate due to shear in the margins reaches 0.01 yr^{-1}, substantially higher than the value of 0.002 yr^{-1} required for crevassing in cold firn [*Vornberger and Whillans*, 1990], there is no evidence in high-resolution SAR or SPOT visible-band imagery of significant crevassing in this area. It is possible that crevasses in these areas are buried, as there are several lines of evidence which suggest that accumulation may be enhanced in the margins, as discussed in section 6.

6. Dynamically Supported Topography

6.1. Margins

The measurement of the two horizontal components of the ice flow velocity using interferometry makes it possible to directly estimate the local vertical strain rate, or rate of flow-driven thinning. If the two horizontal components of the velocity field are u and v (in the x and y directions), and the vertical component is w (in the z direction), continuity requires that

$$\frac{\partial u}{\partial x} + \frac{\partial v}{\partial y} + \frac{\partial w}{\partial z} = 0, \qquad (2)$$

or equivalently that the vertical strain rate is related to the horizontal divergence of the velocity field:

$$\frac{\partial w}{\partial z} = -\left(\frac{\partial u}{\partial x} + \frac{\partial v}{\partial y}\right). \qquad (3)$$

In the high-resolution SPOT visible-band image and SAR image in Plate 2, as well as in the AVHRR-enhanced elevation model (Figure 1a), the sharp southeastern margin of the widening section appears as a narrow trough that is coincident with the large increase in flow speed as ice is added from the southeast side. The location of this trough corresponds to the location of the highest values of flow-driven thinning, derived from the divergence of the INSAR-measured surface velocity field. Plate 2 shows the vertical strain rate over the upper ice stream expressed as the rate of thinning per kilometer of ice thickness (equivalent to the vertical strain rate x 10^3). The peak rate of flow-driven thinning in the marginal trough is 2 m per year per kilometer of ice thickness. The ice in this area is about 3 km thick, but the high horizontal strain rates may not extend through the entire thickness of the ice. It is likely that the upper half of the ice is experiencing this strain rate, leading to thinning of meters per year.

We can use the ice flow measured by SAR interferometry to estimate the scale of dynamic topography in this area. Plate 3a shows 40 flow lines traced upstream through the start of the widening section of the stream. The markers on the flow lines are separated by 250 years of displacement in the present surface velocity field. We have integrated the vertical strain rate (equation (2)) upstream along these flow lines to produce an estimate of the dynamically generated total vertical strain for the area outlined by the green box in Plate 3a. This calculation assumed no initial strain across the downstream profile, which is equivalent to saying that the strain across flow at this downstream profile is zero, or for the purpose of determining the dynamically generated surface topography that the ice stream is flat across flow. The resulting total strain upstream of the lowest profile is displayed as a surface in Plate 3b, shown looking in the direction of the black arrow in Plate 3a. This surface shows a strongly
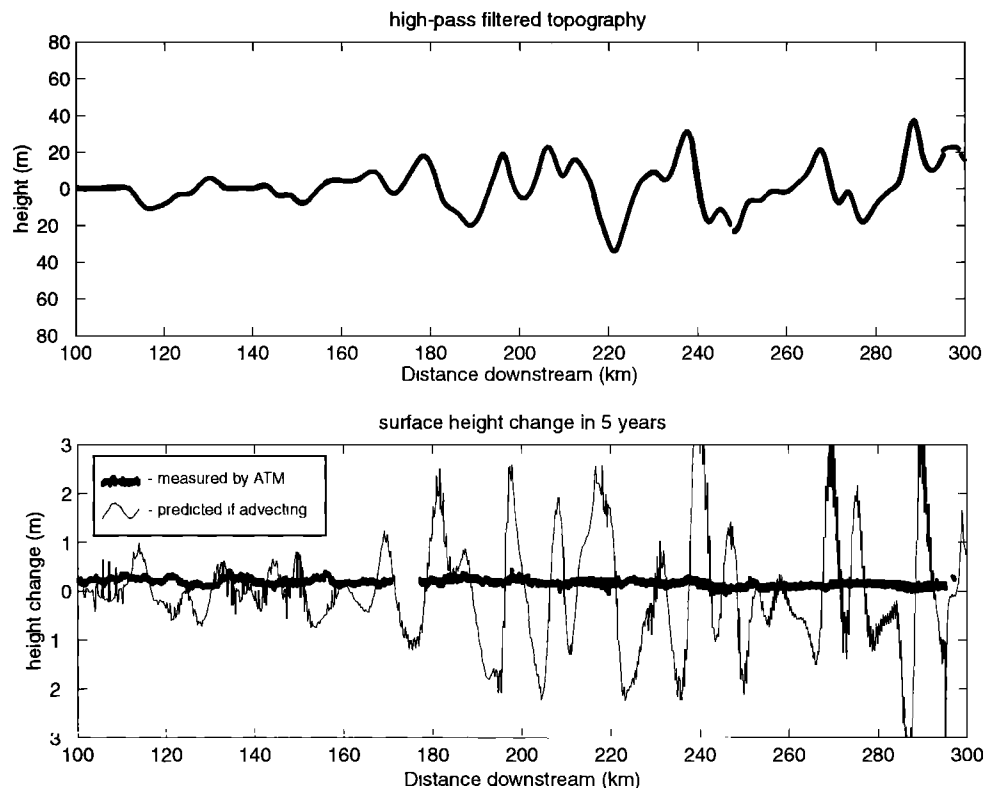
Figure 3. (top) Undulations present along the centerline of the ice stream in the upper reach, as measured by the ATM laser altimeter. The regional slope has been removed with a 30 km high-pass filter. (bottom) Change in height of the surface along this profile over 5 years measured by the ATM laser (about 20 cm) and the amount of height change that would be expected if the topography had been advecting at the ice flow speed.

developed marginal trough on the south side of the stream (to the left in the plate) which is 2-3 km wide, linear, and shows a nearly constant maximum total strain of -0.1. This number is very high, reflecting a total dynamic trough depth of 200-300 m in ice 3 km thick (300 m is a maximum and would be lowered by any reduction in horizontal strain rate with depth). The laser elevation profiles we have for this area show a depth of several tens of meters for the trough and a width of < 2 km (Plate 2 profiles A and B). The profile of the total vertical strain surface corresponding to the left end of cross-flow elevation profile (A) is compared with that laser elevation profile in Plate 3c. While the strain surface in Plate 3b is not representative of the true topography, as we have not included the bed geometry in the analysis, the dynamically generated marginal trough is well represented. The difference between the several hundred meter deep trough predicted by ice flow and the 20 m deep trough measured by the altimeter may be explained by enhanced accumulation due to snow drift over the ~100 years it takes for ice to cross the feature. The low backscatter in the trough in the SAR image in Plate 2 could be produced by this enhanced accumulation rate, as rapid burial reduces the amount of alteration in the firn; the lack of visible crevassing in this area of high shear strain rates may also be due to bridging caused by this enhanced accumulation.

6.2. Surface Undulations

A laser altimeter profile of the surface undulations present in the upper 200 km of the stream is shown in Figure 3. These undulations are also visible in the elevation model of Figure 1a. The ATM laser altimeter flew over the ice stream in 1994 and again in 1999 [*Krabill et al.*, 2000]. While it is commonly assumed that this scale of surface undulation (5-10 km

wavelength, a few to 40 m amplitude) is produced by the flow of ice over obstructions at the bed and so should be fixed in space, the ATM flights give us the opportunity to demonstrate that the undulation-scale topography does indeed have a spatially fixed geometry. The bottom plot in Figure 3 shows the change in surface height over 5 years measured by the ATM laser (thick line) and the amount of height change that would have occurred if the undulations had been advecting with the ice in the stream (determined by multiplying the surface slope along the profile by the ice flow speed). The measured height change is remarkably stable at about 20 cm thickening over the period, independent of position within the undulations. The pattern of height change clearly rules out the advection of the undulation-scale features. The small variations in surface height change across any of the undulations (less than 3 cm in 5 years in the worse case) reflects the fact that accumulation across these undulations is in balance with the deformation caused by ice flow to better than 0.6 cm/yr in snow-equivalent units (so to better than a few millimeters per year water equivalent). This is remarkable given the evidence of large variations in accumulation across surface undulations in other areas [e.g., *Black and Budd*, 1964; accumulation at TUNU, *E. Mosley-Thompson et al.*, this issue]; this argues for a balance between spatial variations in accumulation and the advection of this spatial variation through the undulations so that the surface shape of the ice sheet remains constant except for a uniform thickening.

7. Flow Mechanism

Figure 4 shows two ice-penetrating radar profiles from the University of Kansas coherent ice-sounding radar [*Gogineni et al.*, 1998]. These profiles show the bed reflection, ice thickness with an accuracy of about 10 m, and internal reflectors in the ice. The
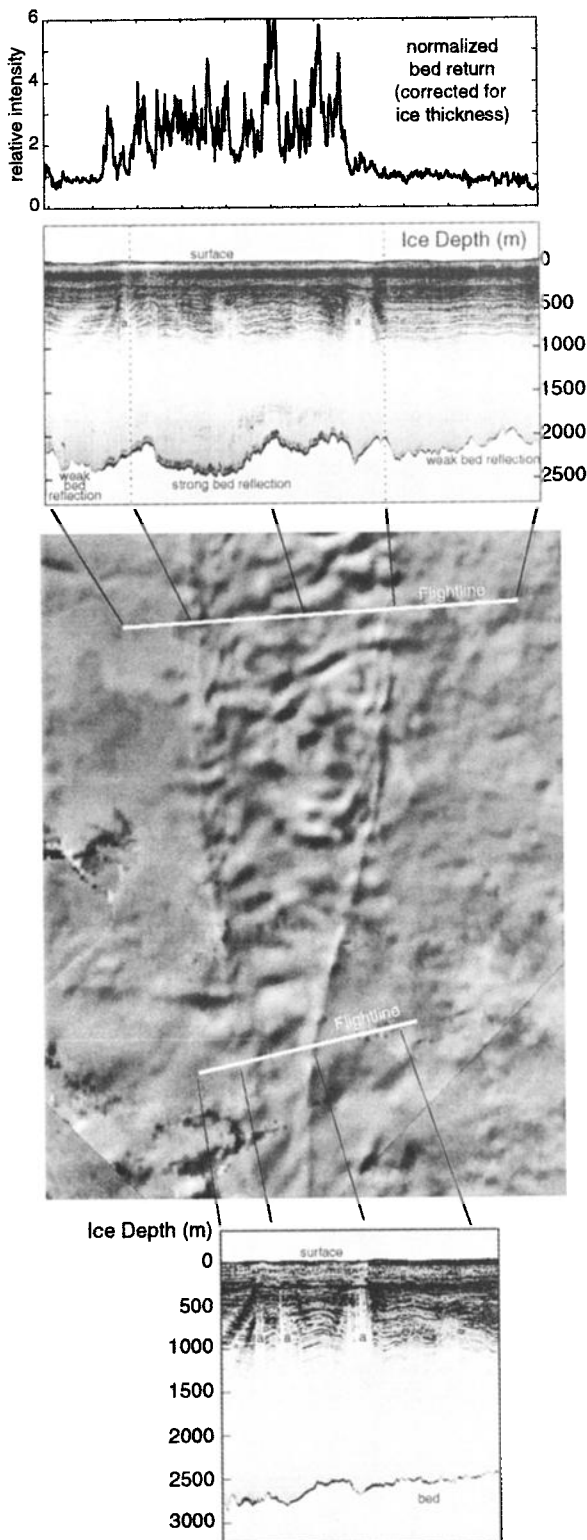
Figure 4. Two ice-penetrating radar profiles across the ice stream, with corresponding flight lines plotted over an enhanced AVHRR image of the stream. The relative strength of the bed reflection in the top profile is plotted at the top of the figure, showing the large contrast between conditions under the stream and adjacent to it.

downstream profile at the top of the figure shows a strongly enhanced bed reflection under the ice stream, and weaker reflections to either side; the relative strength of the bed reflection, corrected for ice thickness, is also plotted, showing that there is a

two to sixfold increase in the bed reflection under the ice stream along this profile. There are strong bed reflections in the upstream profile as well, but they are not confined to the area under the stream. In his model-based analysis of basal temperatures in Greenland, *Huybrechts* [1996] shows two regions, one in the northeast and one in the west, where substantial parts of the bed are at the melting point under present conditions. The area of basal melting in the northeast covers the lower half of the ice stream under most of the simulations in the paper and covers all of the ice stream in the simulation using 125% of the assumed background geothermal heat flux. In the interglacial reference run the bed below the upper half of the ice stream is within a few degrees of the pressure melting point. Since publication of this work, there has been a downward revision of the accumulation rates in northeast Greenland (see papers in this issue) which would lower the effect of advective cooling in the Huybrechts analysis and thus raise the basal temperature, increasing the likelihood that the bed is at the melting point in this basin.

In the downstream profile, there is significant bed topography, with a 300-400 m deep channel occupying the left half of the stream. It is this channel that is responsible for the change in style of the flow profiles (from plug flow to parabolic) which was discussed in the section 6 (Figure 2a, profiles 9 and 10).

8. Conclusions and Discussion

We have presented a series of data sets that illustrate the effects on ice sheet surface topography and ice motion produced by the ice stream in northeast Greenland. A summary of the conclusions that can be drawn from these data sets includes the following:

1. The onset of organized flow occurs within 100 km of the ice divide, as seen from both surface topographic features (marginal troughs, undulations), and INSAR velocities; organized flow may reach even closer to the divide, but it is not expressed in the surface topography, and the areas closer to the divide were not covered by the INSAR measurements.

2. The flow in the upper half of the stream is organized into a single current (and a subtle southern tributary) which is defined by marginal troughs that coincide with regions of measured localized shear. These margins do not show open crevassing until flow speeds in the stream reach 100 m/yr.

3. The patterns of shear in the margins of the upper reach are consistent along the upper 300 km of the stream; the shear margins maintain a relatively constant width and magnitude in spite of changes in the stream width and speed. Shear in the margins in the narrow upper part of the stream reaches the stream center, indicating that a significant fraction of the driving stress for the stream is held from the sides at this point. Downstream, where the width of the stream has increased, the patterns of margin shear do not change, and the shear strain rates toward the stream center are low and variable, indicating a significant resistance to flow at the bed and the balancing of driving stress by both the margins and the basal drag. These conclusions match the results of modeling discussed by *Joughin et al.* [this issue].

4. Ice flow patterns as measured with INSAR are responsible for the marginal troughs and surface undulations within the stream; however, the dynamic topography predicted by ice flow in the marginal troughs is an order of magnitude larger than the troughs measured by laser altimetry. We attribute the difference to local high accumulation (drift) in the trough driven by the topography.

5. Ice flow conditions in the marginal troughs are unlike anything yet documented for the interior of an ice sheet; flow features formed by changing bed conditions would be expected to be 3-5 times the ice thickness (10 km) across, but here the margins are only a few kilometers across. This may reflect changes in ice properties (shear heating?), or some other process.

6. The undulating surface topography of the interior of the stream is not advecting with the ice; in addition, repeated laser

profiles separated by 5 years show less than 5 cm difference in surface height change across the undulations (less than 1 cm/yr), indicating that the undulations are fixed in space and have a constant form, in spite of any possible spatial variations in accumulation.

7. One ice-penetrating radar profile across the stream shows enhanced returns from the bed of the ice stream (2-6 times the return from the bed outside of the stream), consistent at this location with the stream position being determined by a freeze/thaw boundary.

8. Changes in ice stream width in the upper half of the stream are accomplished through the addition of ice across the stream margins, rather than through spreading of flow within the stream. In the wedge-shaped widening region the shear margins are at an angle to the ice flow direction because of the rapid addition of ice to the stream from the sides; this means that the linear nature of the margins in this section is not due to simple lateral shear but may represent some other process.

Ice flow in the interior portions of the ice stream is unique in a number of respects; it probably reflects an interaction with conditions at the bed that is also unique. The geometry of the onset and widening section and the rapid thinning in the margins as ice accelerates into the stream are unique to this ice stream. It is difficult to conceive of an explanation for the localized onset of enhanced flow at such low flow speeds, and so close to the present divide, without appealing to localized heating at the bed. The large differences in flow speed and the well-developed, localized marginal shear suggest that basal ice conditions change from frozen to sliding at discrete boundaries; there is little evidence, except for the southern enhanced-flow-speed region, of any transition zone. While we believe it likely that the organized flow may have its origins in localized heating at the bed, we do not yet have direct evidence for this.

An overview of the stream shows that it flows down a low point in the regional topography and provides what must be the longest discharge path for ice in Greenland, from the northern side of the summit dome to the sea nearly 800 km away. Because the ice stream in northeastern Greenland has had an influence on the surface topography of the ice sheet in the onset region, it is clearly not a short-lived phenomenon. Until we understand the origin of the enhanced ice flow, we will not know the full implications the stream holds for the past history and future discharge of the ice in Greenland.

References

Bamber, J. L., S. Ekholm, and W. Krabill, The accuracy of satellite radar altimeter data over the Greenland ice sheet determined from airborne laser data, Geophys. Res. Lett., 25(16), 3177-3180, 1998.

Bamber, J. L., R. L. Layberry and S. P. Gogineni, A new ice thickness and bed data set for the Greenland ice sheet, 1, Measurement, data reflection, and errors, J. Geophys. Res., this issue.

Bentley, C. R., Antarctic ice streams–A review, J. Geophys. Res., 92, 8843-8858, 1987.

Bindschadler, R., X. Chen, and P. Vornberger, The onset area of Ice Stream D, West Antarctica, J. Glacio., 46(152), 95-101, 2000.

Black, H. P., and W. Budd, Accumulation in the region of Wilkes, Wilkes Land, Antarctica, J. Glaciol., 5(37), 3-15, 1964.

Echelmeyer, K. A., W. D. Harrison, C. Larsen, and J. E. Mitchell, The role of the margins in the dynamics of an active ice stream, J. Glaciol., 40(136), 527-538, 1994.

Ekholm, S., R. Forsberg, and J. M. Brozena, Accuracy of satellite altimeter elevations over the Greenland ice sheet, J. Geophys. Res., 100, 2687-2696, 1995.

Ekholm, S., K. Keller, J. L. Bamber, and S. P. Gogineni, Unusual surface morphology from digital elevation models of the Greenland ice sheet, Geophys. Res. Lett., 25(19), 3623-3626, 1998

Fahnestock, M., R. Bindschadler, R. Kwok, and K. Jezek, Greenland ice-sheet surface-properties and ice dynamics from ERS-1 SAR imagery, Science, 262(5139), 1530-1534, 1993.

Gogineni, S., T. Chuah, C. Allen, K. Jezek, and R. K. Moore, An improved coherent radar depth sounder, J. Glaciol., 44(148), 659-669, 1998.

Hodge, S.M., and S.K. Doppelhammer, Satellite imagery of the onset of streaming flow of ice streams C and D, West Antarctica, J. Geophys. Res., 101, 6669-6677, 1996.

Huybrechts, P., Basal temperature conditions of the Greenland ice sheet during the glacial cycles, Ann. Glaciol., 23, 226-236, 1996.

Jackson, M., and B. Kamb, The marginal shear stress of Ice Stream B, West Antarctica, J. Glaciol., 43(145), 415-426, 1997.

Joughin, I., R. Kwok, and M. Fahnestock, Estimation of ice-sheet motion using satellite radar interferometry: Method and error analysis with application to Humboldt Glacier, Greenland, J. Glaciol., 42(142), 564-575, 1996.

Joughin, I., M. Fahnestock, S. Ekholm, and R. Kwok, Balance velocities of the Greenland ice sheet, Geophys. Res. Lett., 24(23), 3045-3048, 1997.

Joughin, I., L. Gray, R. Bindschadler, S. Price, D. Morse, C. Hulbe, K. Mattar, and C. Werner, Tributaries of West Antarctic ice streams revealed by RADARSAT interferometry, Science, 286(5438), 283-286, 1999.

Joughin, I., M. Fahnestock, D. MacAyeal, J. L. Bamber, P. Gogineni, Observation and analysis of ice flow in the largest Greenland ice stream, J. Geophys. Res., this issue.

Krabill, W., W. Abdalati, E. Frederick, S. Manizade, C. Martin, J. Sonntag, R. Swift, R. Thomas, W. Wright, and J. Yungel, Greenland ice sheet: High-elevation balance and peripheral thinning, Science, 289(5478), 428-430, 2000.

Legarsky, J., A. Wong, T. Akins, and S. P. Gogineni, Detection of hills from radar data in central-northern Greenland, J. Glaciol., 44(146), 182-184, 1998.

Mohr, J. J., N. Reeh, and S. N. Madsen, Three-dimensional glacial flow and surface elevation measured with radar interferometry, Nature, 391(6664), 273-276, 1998.

Mosley-Thompson, E., J. R. McConnell, R. C. Bales, Z. Li, P.-N. Lin, K. Steffen, L. G. Thompson, R. Edwards, and D. Bathke, Local to regional-scale variability of annual net accumulation on the Greenland ice sheet from PARCA cores, J. Geophys. Res., this issue.

Raymond, C., Shear margins in glaciers and ice sheets, J. Glaciol., 42(140), 90-102, 1996.

Rignot, E. J., S. P. Gogineni, W. B. Krabill, and S. Ekholm, North and northeast Greenland ice discharge from satellite radar interferometry, Science, 276(5314), 934-937, 1997.

Scambos, T. A., and M. A. Fahnestock, Improving digital elevation models over ice sheets using AVHRR-based photoclinometry, J. Glaciol., 44(146), 97-103, 1998.

Scambos, T. A., and T. Haran, An image-enhanced DEM of the Greenland ice sheet, Ann. Glaciol., 34, in press.

Vornberger, P. L., and I. M. Whillans, Crevasse deformation and examples from Ice Stream-B, Antarctica, J. Glaciol., 36(122), 3-10, 1990.

Whillans, I. M., and C. J. van der Veen, New and improved determinations of velocity of Ice Stream-B and Ice Stream-C, West Antarctica, J. Glaciol., 39(133), 483-490, 1993.

M. A. Fahnestock, Earth System Science Interdisciplinary Center, 2207 Computer and Space Sci. Bldg., University of Maryland, College Park, MD 20742-2465. (mark@essic.umd.edu)

S. Gogineni, Radar Systems and Remote Sensing Laboratory, University of Kansas, 2291 Irving Hill Rd., Lawrence, KS 66045. (gogineni@ittc.ukans.edu)

I. Joughin and R. Kwok, Jet Propulsion Laboratory, Mail Stop 300-235, 4800 Oak Grove Drive, Pasadena, CA 91109. (ian@rgps1.jpl.nasa.gov, ron@radar-sci.jpl.nasa.gov)

T. Scambos, National Snow and Ice Data Center, CIRES, Campus Box 449, University of Colorado, Boulder, CO 80309-0449. (teds@icehouse.colorado.edu)

W. B. Krabill, NASA Wallops Flight Facility, Mail stop 972.0, Wallops Island, VA 23337.